Fieldlike torque driven switching in rare-earth transition-metal alloys

Huiwen Wang [1,3] Pierre Vallobra,[2,3,*] Yong Xu,[1,2] Zhizhong Zhang,[2] Shouzhong Peng,[1,2,3,†] and Weisheng Zhao [1,2,3]
[1]*Fert Beijing Institute, School of Integrated Circuit Science and Engineering, Beihang University, Beijing 100191, China*
[2]*National Key Laboratory of Spintronics, Hangzhou International Innovation Institute, Beihang University, Hangzhou 311115, China*
[3]*Hefei Innovation Research Institute, Beihang University, Hefei 230013, China*

(Received 7 February 2024; revised 7 July 2024; accepted 14 August 2024; published 9 September 2024)

Spin-orbit torque (SOT) has been widely recognized and applied as the most promising approach for magnetic memory, primarily due to its lower energy consumption and longer device lifetime. However, the mechanism of SOT remains controversial in ferrimagnets, particularly regarding the role of fieldlike torque (FLT). This uncertainty arises from the presence of different gyromagnetic ratios of the sublattices, which generates significant variations particularly in the vicinity of the angular momentum compensation point. In this paper, we demonstrate that, in the vicinity of the angular momentum compensation point, FLT can act as a main driving term for magnetization switching in ferrimagnets through rigorous mathematical analysis and ferrimagnetic macrospin simulation. We also provide clear indications about the materials damping factor on how to tailor the magnetic layer where a charge current is injected. These findings shed light on the intricate behavior of SOT in ferrimagnetic systems and pave a way for further advancements in high-performance magnetic memory devices.

DOI: 10.1103/PhysRevB.110.094413

I. INTRODUCTION

In recent years, spin-orbit torque (SOT) has revealed itself as a promising candidate for the next generation of magnetic random-access memories (MRAM), owing to its intrinsic low power consumption and the long lifetime it offers [1–6]. Indeed, the separated read and write channels allow the memory to last longer than in a spin-transfer torque (STT) architecture [7]. While the applications of SOT in ferromagnetic materials have been extensively investigated, further efforts are necessary for the study of their ferrimagnetic counterparts. Rare-earth transition-metals (RE-TM) ferrimagnetic materials possess the characteristic of having separated angular and magnetic compensation points because of the different Landé factors of both sublattices [8]. At the angular compensation point, RE-TM ferrimagnetic materials exhibit faster dynamics when excited by magnetic field or SOT [9–11].

In 2020, the fastest domain wall velocity ever reached with SOT has consequently been reported in a GdFeCo alloy at the angular compensation point [12]. This study focused on the effect of the SOT dampinglike torque (DLT) which is viewed as a conventional method to move a domain wall. More globally, the DLT is often considered as the main term driving the magnetization switching and the domain wall motion in ferromagnetic materials. Once applying this framework to ferrimagnetic materials, most studies also only mentioned the DLT. While the DLT is indeed the main driving force for domain wall motion in homochiral Néel walls due to geometrical considerations [13,14], whether the effect of fieldlike torque (FLT) in ferrimagnetic materials keeps same properties with ferromagnetic materials is unclear and remains controversial.

In this study, we demonstrate that the FLT cannot be dismissed in ferrimagnetic materials under certain conditions. The FLT strongly dominates the switching process in the vicinity of the angular compensation point. Our study is based on a mathematical approach and is corroborated by simulations performed using practical and reasonable parameters of ferrimagnetic thin films. Furthermore, by tuning the material's intrinsic property, the damping factor, we give clear and strong insight on how to achieve faster and more energy efficient SOT magnetization switching in ferrimagnetic materials.

II. THEORETICAL FRAMEWORK

SOT can have various origins such as the spin Hall effect or Rashba-Edelstein effect. In our case, as displayed in Fig. 1(a), a charge current flowing in the x direction is injected into a heavy metal and then creates a vertical spin current due to strong spin-orbit coupling that will ultimately interact with the magnetic moments of the adjacent magnetic layer. A symmetry breaking magnetic field is applied along the x axis. The typical magnetization dynamics of the SOT switching process which consists of two steps is displayed in Fig. 1(b). First, the magnetization aligns along the y axis during the pulse and then relaxes along $-z$ as seen in Fig. 1(c). The scope of this study is to find the conditions to minimize the time t_0 reaching the equilibrium in the first step. The time t_0 is defined in our simulations as the minimum time t fulfilling the conditions $|m_{y,t}| > 0.99$ and for any time $t1 > t$, $|m_{y,t1}| > 0.99$. By knowing the time t_0, it becomes possible to adjust the current pulse settings to improve the energy efficiency in magnetization switching.

*Contact author: pierrevallobra@buaa.edu.cn
†Contact author: shouzhong.peng@buaa.edu.cn

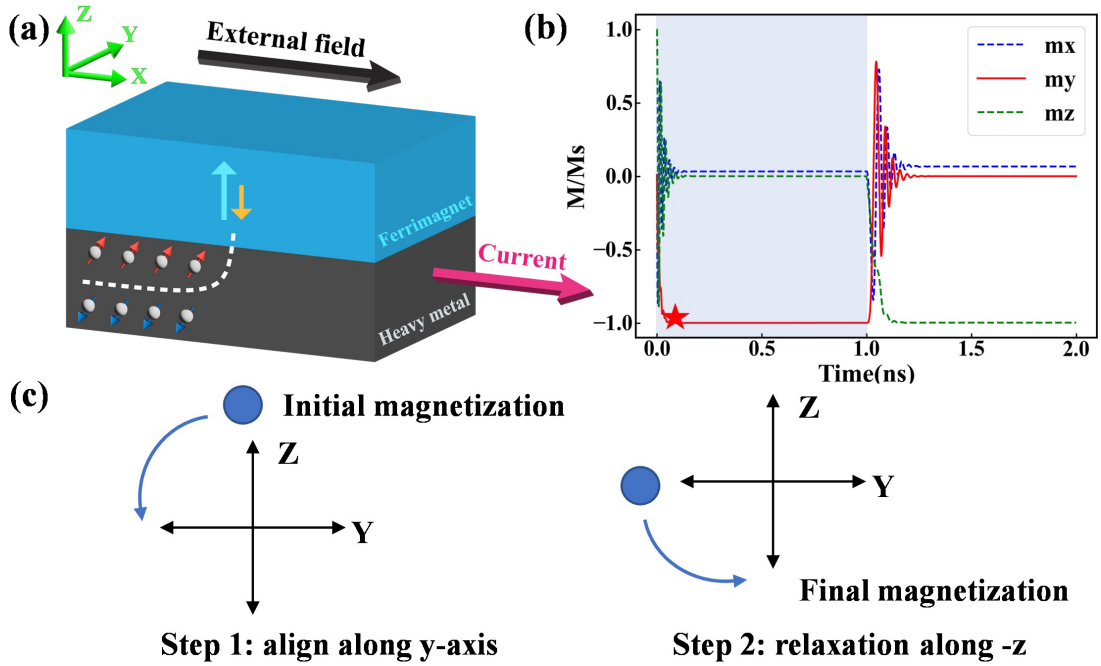

FIG. 1. Standard SOT switching in RE-TM alloys. (a) Schematic of ferrimagnet/heavy metal bilayer during electrical current injection. (b) SOT switching process of $Gd_{44}Co_{56}$ for a 1-ns pulse with current density of 100 MA/cm^2 at room temperature and magnetic damping $\alpha = 0.005$. (c) Step 1 of SOT switching: During the current pulse, the magnetization direction of RE-TM alloys aligns towards the y axis. Step 2 of SOT switching: After the pulse, the magnetization direction of RE-TM alloys relaxes along $-z$.

To understand the process of SOT switching in RE-TM alloys, we first develop the mathematical framework describing the magnetization dynamics derived from ferromagnetic materials. The key parameters of the chosen materials and the default settings are recorded in Supplemental Material Notes 1 and 2 [15], respectively. We consider a macrospin model consisting of two sublattices, TM and RE, with antiparallel alignment. For a sublattice i ($i = 1$ for TM, $i = 2$ for RE), the LLG equation can be written as [16–18]

$$\frac{d\boldsymbol{m_i}}{dt} = -\frac{\gamma_i}{1+\alpha_i^2}[\boldsymbol{m_i} \times \boldsymbol{H}_{\mathbf{eff},i} + \alpha_i \boldsymbol{m_i} \times (\boldsymbol{m_i} \times \boldsymbol{H}_{\mathbf{eff},i})], \quad (1)$$

where the sublattice's magnetization $\boldsymbol{M_i} = M_{s,i}\boldsymbol{m_i}$, $M_{s,i}$ is its magnitude, $\gamma_i = g_i\mu_B/\hbar$ is the gyromagnetic ratio, g is the Landé g factor, μ_B is the Bohr magneton, $\hbar$ is the reduced Planck constant, and α_i is the magnetic damping factor. The effective field includes the in-plane external field $\boldsymbol{H}_{\mathbf{ext},i} = H_{\mathrm{ext},i}\,\boldsymbol{e_x}$, the out-of-plane anisotropy field $\boldsymbol{H}_{k,i} = \frac{2K_{u,i}}{M_{s,i}} m_z \boldsymbol{e_z}$, the local exchange field $\boldsymbol{H}_{\mathbf{ex},i} = h\,\boldsymbol{M}_j$ $(i \neq j)$ with h being the local exchange constant, the dampinglike field $\boldsymbol{H}_{\mathbf{DL},i} = H_{\mathrm{DL},i}(\boldsymbol{\sigma} \times \boldsymbol{m_i})$ and the fieldlike field $\boldsymbol{H}_{\mathbf{FL},i} = H_{\mathrm{FL},i}\boldsymbol{\sigma}$.

In the case of SOT generated by spin Hall effect, the polarization vector is $\boldsymbol{\sigma} = (0, -1, 0)$. The effective field strengths for DLT and FLT are given by [19–23]

$$H_{\mathrm{DL},i} = \frac{j_c \hbar \theta_{\mathrm{SH},i}}{2eM_{s,i}t}, \quad (2)$$

$$H_{\mathrm{FL},i} = \eta H_{\mathrm{DL},i}, \quad (3)$$

where j_c is the current density, $\theta_{\mathrm{SH},i}$ is the spin Hall angle from sublattice i, e is the electron charge, t is the thickness of the ferrimagnetic layer, and η is the ratio between H_{DL} and H_{FL}.

Upon combining the LLG equations for both sublattices magnetization dynamics, we can deduce the following expression for the magnetization of RE-TM alloys, where the net magnetization $\boldsymbol{M} = M_s\boldsymbol{m}$ ($M_s = M_{s1} - M_{s2}$, $\boldsymbol{m} = \boldsymbol{m}_1 = -\boldsymbol{m}_2$):

$$\frac{d\boldsymbol{m}}{dt} = -\frac{\gamma'}{1+\alpha'^2}[\boldsymbol{m} \times \boldsymbol{H}_{\mathbf{eff}} + \alpha' \boldsymbol{m} \times (\boldsymbol{m} \times \boldsymbol{H}_{\mathbf{eff}})]. \quad (4)$$

To maintain the same form for Eq. (4) as in Eq. (1), we introduce the modified gyromagnetic ratio $\gamma' = \frac{M_s}{S}$ and damping $\alpha' = \frac{S_0}{S}$. The spin momentum S, S_0 and the effective field $\boldsymbol{H}_{\mathbf{eff}}$ have the following expressions, respectively:

$$S = \frac{M_{s1}}{\gamma_1} - \frac{M_{s2}}{\gamma_2}, \quad (5)$$

$$S_0 = \alpha_1 \frac{M_{s1}}{\gamma_1} + \alpha_2 \frac{M_{s2}}{\gamma_2}, \quad (6)$$

$$\boldsymbol{H}_{\mathbf{eff}} = \boldsymbol{H}_{\mathbf{ext}} + \boldsymbol{H}_k - (p_1 + p_2)\boldsymbol{H}_{\mathbf{DL}} - (p_1 - p_2)\boldsymbol{H}_{\mathbf{FL}}. \quad (7)$$

Without loss of generality, we consider that both sublattices have the same damping value ($\alpha = \alpha_1 = \alpha_2$). Different damping constants can also be accommodated in this model [24], as further developed in Supplemental Material Note 3 [15]. $\boldsymbol{H}_{\mathbf{ext}} = 10mT\,\boldsymbol{e_x}$, $H_k = \frac{2K_u}{\mu_0 M_s} m_z \boldsymbol{e_z}$, $K_u = K_{u1} + K_{u2}$. Regarding the total effective local exchange field, the contributions from both sublattices cancel each other out in the final LLG equation since they share the same exchange constant h, due to the reciprocity of the exchange. Additionally, a typical estimated temperature independent value of the exchange interaction is $C_{\mathrm{ex}} = \mu_0 h M_{\mathrm{TM}} M_{\mathrm{RE}} = 36$ kJ/m^3 [25]. Due to this high value of the intersublattice coupling, we consider both sublattices to be strictly antiparallel. $\boldsymbol{H}_{\mathbf{DL}} = \frac{j_c \hbar \theta_{\mathrm{SH}}}{2eM_s t}(\boldsymbol{\sigma} \times \boldsymbol{m})$

and $\boldsymbol{H}_{\mathbf{FL}} = \eta \frac{j_c \hbar \theta_{\mathrm{SH}}}{2eM_s t} \boldsymbol{\sigma}$ are dependant on the total magnetization M_s in the effective field $\boldsymbol{H}_{\mathbf{eff}}$.

Furthermore, each sublattice absorbs a portion p_i of the spin current such that ($\theta_{\mathrm{SH},i} = p_i \theta_{\mathrm{SH}}$, $p_1 + p_2 = 1$) [25,26]. We now apply this framework to the case of a RE-TM alloy by considering index 1 attached to the TM sublattice and index 2 attached to the RE sublattice. This model enables researchers to incorporate sublattice absorption terms while preserving the intrinsic properties of RE-TM alloys, as explored in Supplemental Material Note 4 [15]. Since $4f$ magnetic moments interact very little with spin currents, we consider $p_1 = 1$ and $p_2 = 0$. In other words, we consider that the SOT torques are acting solely on the transition metal because it is the element absorbing most of the spin current.

For convenience, we introduce two parameters γ_{eff} and α_{eff} to represent certain combinations of the modified gyromagnetic ratio γ' and Gilbert damping parameter α'. Specifically, we define them as

$$\gamma_{\mathrm{eff}} = \frac{\gamma'}{1 + (\alpha')^2}, \tag{8}$$

$$\alpha_{\mathrm{eff}} = \frac{\gamma' \alpha'}{1 + (\alpha')^2}. \tag{9}$$

Upon developing Eq. (4), these two parameters γ_{eff} and α_{eff} allow us to write in a concise way. It is worth noting that the initial magnetic damping α remains constant across all temperatures [27], not varying with the temperature [9]. The variation of α' influences the updated physical characteristics of α_{eff}. The four SOT related terms are shown in the following:

$$d\boldsymbol{m}_{\mathbf{DL}} = -\gamma_{\mathrm{eff}} H_{\mathrm{DL}} \boldsymbol{m} \times (\boldsymbol{\sigma} \times \boldsymbol{m}), \tag{10}$$

$$d\boldsymbol{m}_{\mathbf{FL}} = -\gamma_{\mathrm{eff}} H_{\mathrm{FL}} \boldsymbol{m} \times \boldsymbol{\sigma}, \tag{11}$$

$$d\boldsymbol{m}^{\boldsymbol{\alpha}}_{\mathbf{DL}} = -\alpha_{\mathrm{eff}}\, H_{\mathrm{DL}} \boldsymbol{m} \times \boldsymbol{\sigma}, \tag{12}$$

$$d\boldsymbol{m}^{\boldsymbol{\alpha}}_{\mathbf{FL}} = -\alpha_{\mathrm{eff}}\, H_{\mathrm{FL}} \boldsymbol{m} \times (\boldsymbol{m} \times \boldsymbol{\sigma}). \tag{13}$$

While both $d\boldsymbol{m}_{\mathbf{FL}}$ and $d\boldsymbol{m}^{\boldsymbol{\alpha}}_{\mathbf{DL}}$ trigger precession around the polarization vector, $d\boldsymbol{m}_{\mathbf{DL}}$ and $d\boldsymbol{m}^{\boldsymbol{\alpha}}_{\mathbf{FL}}$ align the total magnetization along $\boldsymbol{\sigma}$. To examine the respective contributions of each torque on the switching process in ferrimagnetic materials, it is essential to specifically focus on the terms $d\boldsymbol{m}_{\mathbf{DL}}$ and $d\boldsymbol{m}^{\boldsymbol{\alpha}}_{\mathbf{FL}}$.

Since the expressions of the four SOT terms are derived from the LLG equation, they are also present in the cases of ferromagnets. In ferromagnetic materials, $d\boldsymbol{m}^{\boldsymbol{\alpha}}_{\mathbf{FL}}$ is mostly not taken into account because its amplitude is far less than $d\boldsymbol{m}_{\mathbf{DL}}$ due to the small and unchanged damping α_{eff} value. Conversely, in RE-TM alloys, α_{eff} undergoes significant alterations due to the intersublattice competition. For instance, α' diverges at the angular compensation point, leading to a substantial variation of α_{eff}. It opens up the possibility for RE-TM ferrimagnets to experience faster SOT switching.

Using the macrospin model, we simulated the SOT switching for the most prevalent ferrimagnetic materials at different current densities and extracted the corresponding values of t_0 as shown in Fig. 2(a). The 1 ns rectangular current pulse is taken into observation.

The material parameters at 300 K are detailed in Supplemental Material Note 1. The materials considered are $Gd_{23.5}Fe_{60.9}Co_9$ [8,27–29], $Gd_{44}Co_{56}$ [30], $Tb_{24}Co_{76}$ [26,31–34], $Dy_{26.5}Co_{73.5}$ [35–40], and $Ho_{32.5}Co_6$ [35–38,41,42].

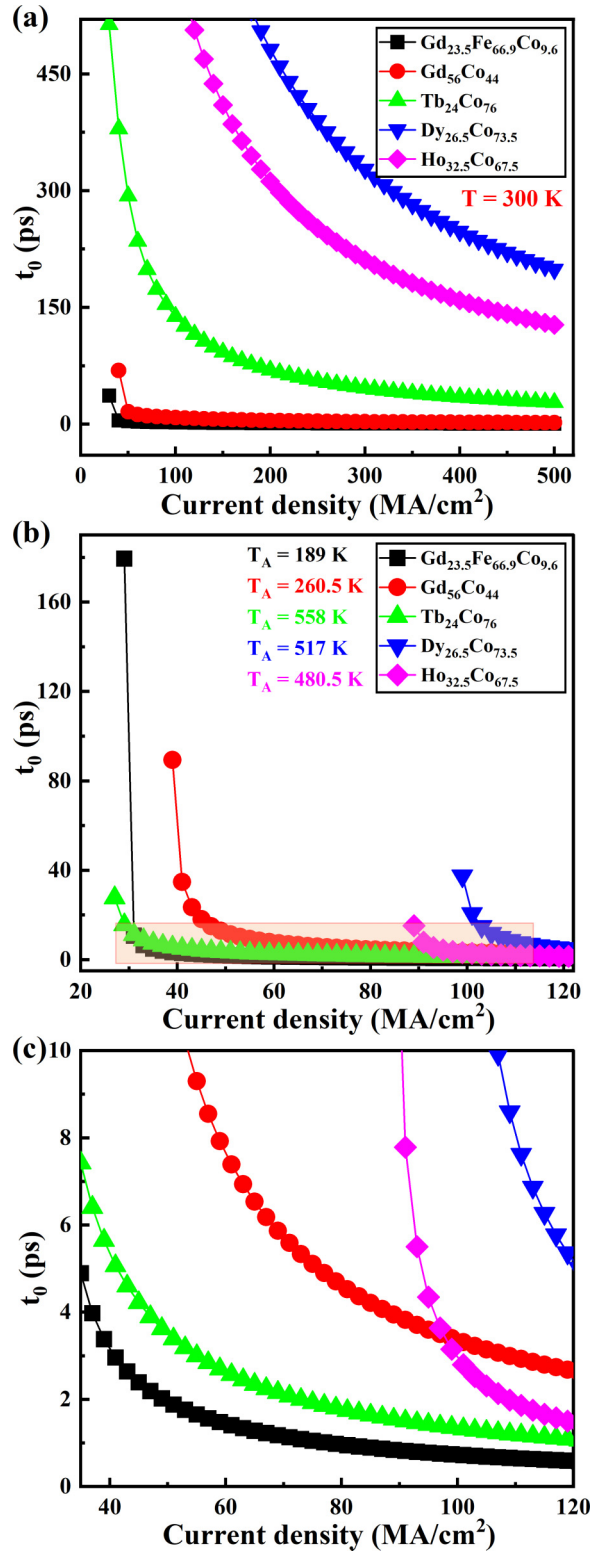

FIG. 2. Choosing a promising candidate among RE-TM alloys: (a) Evolution of t_0 with current density at room temperature for different alloys and (b) at the angular momentum compensation temperature for each material. (c) The enlarged view in case (b).

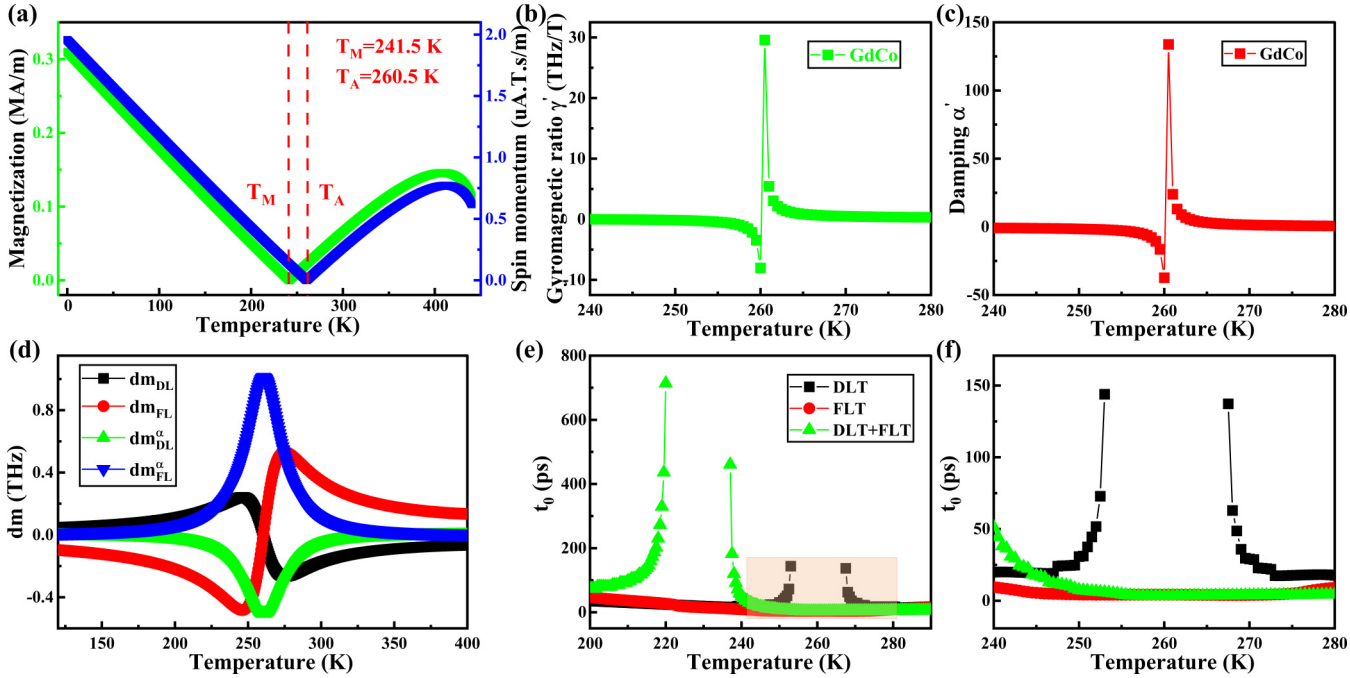

FIG. 3. Magnetic properties of $Gd_{44}Co_{56}$: (a) Magnetization and spin momentum at different temperatures. (b) Modified gyromagnetic ratio γ' and (c) damping α' at different temperatures. (d) Magnitude of four SOT related terms at different temperatures. (e) Switching time t_0 at different temperatures for three cases: (1) only considering DLT, (2) only considering FLT, and (3) considering both DLT and FLT together. (f) Partial enlarged graph of (e).

For each ferrimagnetic alloy, we observe a strong effect of the current density on the switching time t_0. The time t_0 decreases accompanied by the increasing current density. Because of the dependence of the SOT torques on the modified terms γ' and α', there are obvious differences of t_0 values among the different materials. For each material investigated, we change its temperature from room temperature to its own angular compensation temperature (T_A). All values of t_0 at T_A are sizably smaller than at 300 K as shown in Figs. 2(b) and 2(c). The switching time t_0 can even reach a value as low as 2 ps at low current density for $Gd_{23.5}Fe_{60.9}Co_9$ and $Tb_{24}Co_{76}$. However, 189 K is too low and 558 K is too high for practical applications. Thus, selecting a material that has an angular compensation close to room temperature is more suitable. Because of $Gd_{44}Co_{56}$ angular compensation temperature in the proximity of room temperature, we chose it to conduct further investigations. For $Gd_{44}Co_{56}$, the key material parameters are as follows: $K_u = 25\text{kJ/m}^3$, $g_{Gd} = 2$, $g_{Co} = 2.05$, $\theta_{SH} = 0.155$.

Furthermore, $Gd_{44}Co_{56}$ has been a natural candidate for experimental studies involving angular compensation. It is also noteworthy that the angular compensation temperature can be adjusted by changing the material's stoichiometry, providing greater flexibility to tailor the material properties. However, for each Re_xTM_{1-x} alloy, above and below certain x threshold values, the anisotropy lies in-plane. This limits the number of RE-TM materials that simultaneously have angular compensation points around room temperature and can be used in a device with perpendicular magnetic anisotropy.

$Gd_{44}Co_{56}$ magnetic properties are shown in Figs. 3(a)–3(c); at T_A, the modified gyromagnetic ratio γ' and damping α' rapidly diverge to infinity which mainly results in the four SOT related terms' amplitude varying sizably. We observe, as expected, a divergence at T_A for both γ' and α'. The amplitude associated with each SOT term is shown in Fig. 3(d). Strikingly, the two α related terms peak at the angular compensation point while the two other terms cancel at this temperature. It clearly demonstrates that, contrary to the ferromagnetic case, the fieldlike term cannot be neglected in RE-TM ferrimagnetic alloys, especially in the vicinity of the angular compensation point. In addition, the full magnetization switching can be achieved solely by the FLT, as shown in more detail in Supplemental Material Note 5 [15]. To further confirm the role of the FLT term compared to the DLT term, we plot for $Gd_{44}Co_{56}$ in Figs. 3(e) and 3(f) the value of t_0 in the case where only FLT is applied, only DLT is applied, and both are applied.

Coherently with the norm of each $\boldsymbol{dm}$ term, at the angular compensation point t_0 is highly reduced for the FLT case and diverges for the DLT case. Furthermore, t_0 seems to be at a minimum at the angular compensation point—the switching is fast not only in the direct vicinity of T_A, but in a wide window of temperatures around 40 K. Interestingly there is a temperature (229 K) at which t_0 diverges when both torques are present. At this temperature, $d\boldsymbol{m}^{\alpha}_{\mathbf{FL}}$ and $d\boldsymbol{m}_{\mathbf{DL}}$ exactly cancel each other out, as can be seen by the crossing of the corresponding curves in Fig. 3(d). For real applications, it is important to know how fast the switching can be and also how narrow the conditions are to obtain this fast switching. Moreover, we choose $Tb_{24}Co_{76}$ as another example to demonstrate that our analysis applies across the entire range of RE-TM alloys, with details provided

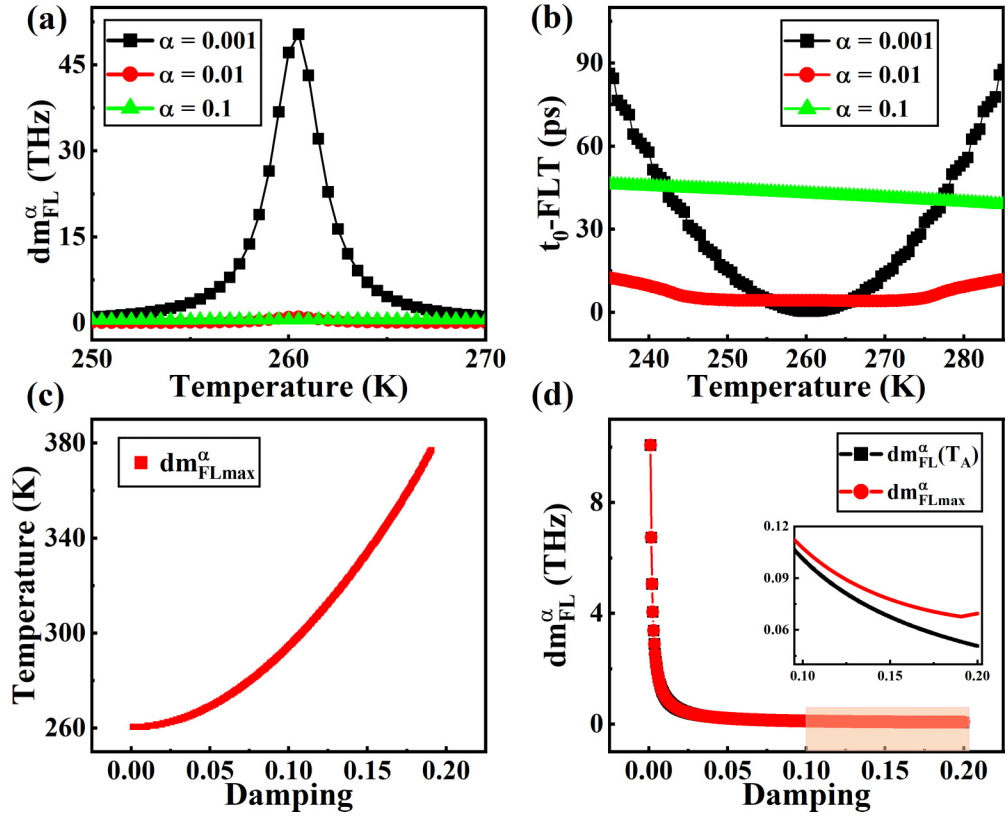

FIG. 4. Effects of the damping constant on the of $Gd_{44}Co_{56}$ properties: (a) Amplitude of dm^{α}_{FL} varied with temperature. (b) Switching time t_0 changed with damping factor when only FLT is present. (c) Temperature T_{max}, corresponding to the peak of the dm^{α}_{FL}, varied with the increasing damping constant α. (d) Comparison of dm^{α}_{FL} at T_A and T_{max}.

in Supplemental Material Note 6 [15]. To test the robustness of our model, we performed micromagnetic simulations in $Gd_{44}Co_{56}$ as detailed in Supplemental Material Note 7 [15]. These simulations support the hypothesis of coherent dynamics of the magnetic moment and confirm the effects of the FLT and of the DLT around the angular compensation point.

Since in the same alloy the damping constant can change the material physical properties and strongly depends on the growth conditions, we studied the effect of varying damping constants on the SOT switching solely driven by FLT. Thus, to gain insight into the possible window of operation for fast SOT switching, we studied the role of the damping constant as observed in Fig. 4.

As shown on Fig. 4(a), the norm of $d\boldsymbol{m}^{\boldsymbol{\alpha}}_{\mathbf{FL}}$ is plotted as a function of the temperature for three different values of the damping factor. While it could be at first expected that the dm^{α}_{FL} increases with the damping constant, the opposite situation actually occurs in the vicinity of the angular compensation. This is due to the term $1 + (\alpha')^2$ in the denominator of α_{eff}. In ferromagnetic materials, this term is almost equal to 1, contrary to the ferrimagnetic case. It leads to the norm of $d\boldsymbol{m}^{\boldsymbol{\alpha}}_{\mathbf{FL}}$ scaling with $1/\alpha$ for values of α' that are much higher than 1. However, as seen in Fig. 4(a), this comes with a drawback. The peak at angular compensation is higher but also narrower for lower values of α. As observed in Fig. 4(b), the same phenomenon occurs for the switching time t_0, where the switching is faster for lower damping values, but the peak for a damping constant of 0.001 is very narrow. Indeed, if the temperature is only 10 K away from the angular compensation point, it is even more beneficial to have a damping of 0.01 compared to 0.001. Thus, the control of the temperature is a major challenge for low damping constants. Another interesting feature of Fig. 4(b) is that for a higher value of the damping constant ($\alpha = 0.1$) the switching time does not reach a minimum in the vicinity of the angular compensation anymore. This is further confirmed in Fig. 4(c) where we plotted the value of the temperature T_{max} at which the $d\boldsymbol{m}^{\boldsymbol{\alpha}}_{\mathbf{FL}}$ norm is maximum as a function of the damping constant. We observe a shift toward higher temperatures for increasing values of the damping constant. However, this shift is still less than 10 K for realistic damping values, lower than 0.025. We plotted in Fig. 4(d) the norm of the $d\boldsymbol{m}^{\boldsymbol{\alpha}}_{\mathbf{FL}}$ vector as a function of the damping constant for temperature, at T_A and T_{max}. We only observe a negligible difference between the two curves for low damping constants. The difference between the two curves increases with the damping constant as seen in the inset.

III. DISCUSSION

Several criteria for a fast SOT switching in ferrimagnetic RE-TM alloys emerge. First, the operation temperature should be close to the angular compensation temperature. As we mentioned beforehand, GdCo alloys seem to be natural candidates because of their angular compensation point close to room temperature. Furthermore, the sample growth

process should be optimized to reach the lowest damping constant possible in order to maximize the fieldlike torque at the angular compensation. Besides, the dynamic of the relaxation step along $-\mathbf{z}$ after the current is turned down is triggered by the anisotropy related term whose expression is $-\alpha_{\text{eff}}\boldsymbol{m} \times (\boldsymbol{m} \times \boldsymbol{H_k})$. Thus, reducing to a minimum t_0 for the first step also allows for a faster relaxation step once the current is turned down because both steps depend on the value of α_{eff}. This high α_{eff}, which arises from a low magnetic damping constant $\alpha = 0.001$ as shown in Fig. 4, also prevents the back switching from happening by limiting the precession during the relaxation step, similarly to the ferromagnetic cases [43,44]. From an industrial perspective, Joule heating poses a challenge to maintain a constant temperature and stable performances in the large array of devices. Due to the strong dependence of t_0 on the material temperature at low values of the damping constant α, it may be more suitable to tailor materials with intermediate values of α, which could lead to performances that are not optimized in the ideal conditions, i.e., at the precise peak temperature, but rather stable over a wider range of temperature. Besides, concerning the torques themselves, since it is clear that the FLT allows for a faster switching in the vicinity of the angular compensation point, it seems suitable to work with materials having higher values of η. In particular, topological insulators with elevated η ratio are natural candidates [45–47]. Their interface with the ferrimagnetic material should also be strictly scrutinized to avoid interfacial spin current reflection and sizable increase of the damping constant.

IV. CONCLUSION

In summary, we rigorously demonstrated through mathematical analysis and simulations, including the macrospin model and micromagnetic simulations, that fieldlike torque has to be taken into account to precisely describe the SOT switching process of RE-TM ferrimagnetic alloys. In the vicinity of the angular compensation temperature, the fieldlike torque even dominates the switching process, resulting in considerably faster switching times. We offer guidance on the material's damping factor to ensure fast and reliable switching in practical magnetic memory applications, where temperature control is limited. We also provide clear indications on how to tailor both the magnetic layer and the layer into which a charge current is injected. Our results pave the way toward fast and energy efficient next generation magnetic memories.

ACKNOWLEDGMENTS

The authors gratefully acknowledge the support from the National Natural Science Foundation of China (Grants No. 12250410245 and No. 62374013), the Fundamental Research Funds for the Central Universities, the Young Elite Scientists Sponsorship Program by CAST (Grant No. 2021QNRC001), the National Key Research and Development Program of China (Grants No. 2021YFB3601303 and No. 2021YFB3601300).

[1] M. Miron, K. Garello, G. Gaudin, P.-J. Zermatten, M. V. Costache, S. Auffret, S. Bandiera, B. Rodmacq, A. Schuhl, and P. Gambardella, Perpendicular switching of a single ferromagnetic layer induced by in-plane current injection, Nature (London) **476**, 189 (2011).

[2] P. Gambardella and I. M. Miron, Current-induced spin–orbit torques, Philos. Trans. R. Soc. A **369**, 3175 (2011).

[3] K. Garello, F. Yasin, H. Hody, S. Couet, L. Souriau, S. H. Sharifi, J. Swerts, R. Carpenter, S. Rao, W. Kim, J. Wu, K. K. V. Sethu, M. Pak, N. Jossart, D. Crotti, A. Furnémont, and G. S. Kar, in *Manufacturable 300mm Platform Solution for Field-Free Switching Sot-Mram*, Kyoto, Japan Symposium on VLSI Circuits (IEEE, 2019), pp. T194-T195.

[4] S. Peng, D. Zhu, W. Li, H. Wu, A. J. Grutter, D. A. Gilbert, J. Lu, D. Xiong, W. Cai, P. Shafer, K. L. Wang, and W. Zhao, Exchange bias switching in an antiferromagnet/ferromagnet bilayer driven by spin–orbit torque, Nat. Electron. **3**, 757 (2020).

[5] Q. Shao, P. Li, L. Liu, H. Yang, S. Fukami, A. Razavi, H. Wu, K. Wang, F. Freimuth, Y. Mokrousov, M. D. Stiles, S. Emori, A. Hoffmann, J. Åkerman, K. Roy, J.-P. Wang, S.-H. Yang, K. Garello, and W. Zhang, Roadmap of spin-orbit torques, IEEE Trans. Magn. **57**, 800439 (2021).

[6] J. Lu, W. Li, J. Liu, Z. Liu, Y. Wang, C. Jiang, J. Du, S. Lu, N. Lei, S. Peng, and W. Zhao, Voltage-gated spin-orbit torque switching in IrMn-based perpendicular magnetic tunnel junctions, Appl. Phys. Lett. **122**, 012402 (2023).

[7] G. Prenat, K. Jabeur, G. Di Pendina, O. Boulle, and G. Gaudin, Beyond STT-MRAM, Spin Orbit Torque RAM SOT-MRAM for high speed and high reliability applications, *Spintronics-based Computing*, edited by W. Zhao and G. Prenat (Springer, Cham, 2015), pp. 145–157.

[8] Y. Hirata, D.-H. Kim, T. Okuno, T. Nishimura, D.-Y. Kim, Y. Futakawa, H. Yoshikawa, A. Tsukamoto, K.-J. Kim, S.-B. Choe, and T. Ono, Correlation between compensation temperatures of magnetization and angular momentum in GdFeCo ferrimagnets, Phys. Rev. B **97**, 220403(R) (2018).

[9] C. D. Stanciu, A. V. Kimel, F. Hansteen, A. Tsukamoto, A. Itoh, A. Kiriliyuk, and T. Rasing, Ultrafast spin dynamics across compensation points in ferrimagnetic GdFeCo: The role of angular momentum compensation, Phys. Rev. B **73**, 220402(R) (2006).

[10] Y. Zhang, X. Feng, Z. Zheng, Z. Zhang, K. Lin, X. Sun, G. Wang, J. Wang, J. Wei, P. Vallobra, Y. He, Z. Wang, L. Chen, K. Zhang, Y. Xu, and W. Zhao, Ferrimagnets for spintronic devices: From materials to applications, Appl. Phys. Rev. **10**, 011301 (2023).

[11] S. K. Kim, G. S. D. Beach, K.-J. Lee, T. Ono, T. Rasing, and H. Yang, Ferrimagnetic spintronics, Nat. Mater. **21**, 24 (2022).

[12] K. Cai, Z. Zhu, J. M. Lee, R. Mishra, L. Ren, S. D. Pollard, P. He, G. Liang, K. L. Teo, and H. Yang, Ultrafast and energy-efficient spin–orbit torque switching in compensated ferrimagnets, Nat. Electron **3**, 37 (2020).

[13] S. Emori, U. Bauer, S.-M. Ahn, E. Martinez, and G. S. D. Beach, Current-driven dynamics of chiral ferromagnetic domain walls, Nat. Mater. **12**, 611 (2013).

[14] A. V. Khvalkovskiy, V. Cros, D. Apalkov, V. Nikitin, M. Krounbi, K. A. Zvezdin, A. Anane, J. Grollier, and A. Fert, Matching domain-wall configuration and spin-orbit torques for efficient domain-wall motion, Phys. Rev. B **87**, 020402(R) (2013).

[15] See Supplemental Material at http://link.aps.org/supplemental/10.1103/PhysRevB.110.094413 for the models used to obtain the results for common ferrimagnetic alloys from the macrospin model. This includes details of the key parameters of RE-TM alloys, the default settings in the RE-TM model, discussions on the sublattice damping constant and sublattice spin current absorption factor in the RE-TM model, as well as the examination of magnetization switching driven by FLT. Additionally, the performance of $Tb_{24}Co_{76}$ is provided to further validate our findings, with a comparison between microsimulation and our model to demonstrate robustness, which also contains Refs. [8,24–42].

[16] L. Landau and E. Lifshitz, On the theory of the dispersion of magnetic permeability in ferromagnetic bodies, Phys. Z. Sowjetunion **8**, 101 (1935).

[17] T. L. Gilbert, A phenomenological theory of damping in ferromagnetic materials, IEEE Trans. Magn. **40**, 3443 (2004).

[18] H. Oezelt, A. Kovacs, F. Reichel, J. Fischbacher, S. Bance, M. Gusenbauer, C. Schubert, M. Albrecht, and T. Schrefl, Micromagnetic simulation of exchange coupled ferri-/ferromagnetic heterostructures, J. Magn. Magn. Mater. **381**, 28 (2015).

[19] L. Liu, O. J. Lee, T. J. Gudmundsen, D. C. Ralph, and R. A. Buhrman, Current-induced switching of perpendicularly magnetized magnetic layers using spin torque from the spin hall effect, Phys. Rev. Lett. **109**, 096602 (2012).

[20] R. Mishra, J. Yu, X. Qiu, M. Motapothula, T. Venkatesan, and H. Yang, Anomalous current-induced spin torques in ferrimagnets near compensation, Phys. Rev. Lett. **118**, 167201 (2017).

[21] N. Roschewsky, C.-H. Lambert, and S. Salahuddin, Spin-orbit torque switching of ultralarge-thickness ferrimagnetic GdFeCo, Phys. Rev. B **96**, 064406 (2017).

[22] D. Zhu and W. Zhao, Threshold current density for perpendicular magnetization switching through spin-orbit torque, Phys. Rev. Appl. **13**, 044078 (2020).

[23] K. Garello, I. M. Miron, C. O. Avci, F. Freimuth, Y. Mokrousov, S. Blügel, S. Auffret, O. Boulle, G. Gaudin, and P. Gambardella, Symmetry and magnitude of spin–orbit torques in ferromagnetic heterostructures, Nat. Nanotechnol. **8**, 587 (2013).

[24] R. Abrudan, M. Hennecke, F. Radu, T. Kachel, K. Holldack, R. Mitzner, A. Donges, S. Khmelevskyi, A. Deák, L. Szunyogh, U. Nowak, S. Eisebitt, and I. Radu, Element-specific magnetization damping in ferrimagnetic $DyCo_5$ alloys revealed by ultrafast x-ray measurements, Phys. Status Solidi RRL **15**, 2100047 (2021).

[25] G. Sala, C.-H. Lambert, S. Finizio, V. Raposo, V. Krizakova, G. Krishnaswamy, M. Weigand, J. Raabe, M. D. Rossell, E. Martinez, and P. Gambardella, Asynchronous current-induced switching of rare-earth and transition-metal sublattices in ferrimagnetic alloys, Nat. Mater. **21**, 640 (2022).

[26] S.-G. Je, J.-C. Rojas-Sánchez, T. H. Pham, P. Vallobra, G. Malinowski, D. Lacour, T. Fache, M.-C. Cyrille, D.-Y. Kim, S.-B. Choe, M. Belmeguenai, M. Hehn, S. Mangin, G. Gaudin, and O. Boulle, Spin-orbit torque-induced switching in ferrimagnetic alloys: Experiments and modeling, Appl. Phys. Lett. **112**, 062401 (2018).

[27] D.-H. Kim, T. Okuno, S. K. Kim, S.-H. Oh, T. Nishimura, Y. Hirata, Y. Futakawa, H. Yoshikawa, A. Tsukamoto, Y. Tserkovnyak, Y. Shiota, T. Moriyama, K.-J. Kim, K.-J. Lee, and T. Ono, Low magnetic damping of ferrimagnetic GdFeCo alloys, Phys. Rev. Lett. **122**, 127203 (2019).

[28] D.-H. Kim, M. Haruta, H.-W. Ko, G. Go, H.-J. Park, T. Nishimura, D.-Y. Kim, T. Okuno, Y. Hirata, Y. Futakawa, H. Yoshikawa, W. Ham, S. Kim, H. Kurata, A. Tsukamoto, Y. Shiota, T. Moriyama, S.-B. Choe, K.-J. Lee, and T. Ono, Bulk Dzyaloshinskii–Moriya interaction in amorphous ferrimagnetic alloys, Nat. Mater. **18**, 685 (2019).

[29] I. Radu, K. Vahaplar, C. Stamm, T. Kachel, N. Pontius, H. A. Dürr, T. A. Ostler, J. Barker, R. F. L. Evans, R. W. Chantrell, A. Tsukamoto, A. Itoh, A. Kirilyuk, T. Rasing, and A. V. Kimel, Transient ferromagnetic-like state mediating ultrafast reversal of antiferromagnetically coupled spins, Nature (London) **472**, 205 (2011).

[30] L. Caretta, M. Mann, F. Büttner, K. Ueda, B. Pfau, C. M. Günther, P. Hessing, A. Churikova, C. Klose, M. Schneider, D. Engel, C. Marcus, D. Bono, K. Bagschik, S. Eisebitt, and G. S. D. Beach, Fast current-driven domain walls and small skyrmions in a compensated ferrimagnet, Nat. Nanotechnol. **13**, 1154 (2018).

[31] S. Alebrand, M. Gottwald, M. Hehn, D. Steil, M. Cinchetti, D. Lacour, E. E. Fullerton, M. Aeschlimann, and S. Mangin, Light-induced magnetization reversal of high-anisotropy TbCo alloy films, Appl. Phys. Lett. **101**, 162408 (2012).

[32] R. F. L. Evans, W. J. Fan, P. Chureemart, T. A. Ostler, M. O. A. Ellis, and R. W. Chantrell, Atomistic spin model simulations of magnetic nanomaterials, J. Phys.: Condens. Matter **26**, 103202 (2014).

[33] J. Finley and L. Liu, Spin-Orbit-Torque efficiency in compensated ferrimagnetic cobalt-terbium alloys, Phys. Rev. Appl. **6**, 054001 (2016).

[34] R. Moreno, T. A. Ostler, R. W. Chantrell, and O. Chubykalo-Fesenko, Conditions for thermally induced all-optical switching in ferrimagnetic alloys: Modeling of TbCo, Phys. Rev. B **96**, 014409 (2017).

[35] F. J. Darnell, Temperature dependence of lattice parameters for Gd, Dy, and Ho, Phys. Rev. **130**, 1825 (1963).

[36] S. Khmelevskyi and P. Mohn, Quantitative theory of Invar-like anomalies in $DyCo_2$ and $HoCo_2$, Phys. Rev. B **66**, 220404(R) (2002).

[37] P. Hansen, S. Klahn, C. Clausen, G. Much, and K. Witter, Magnetic and magnetooptical properties of rareearth transition-metal alloys containing Dy, Ho, Fe, Co, J. Appl. Phys. **69**, 3194 (1991).

[38] N. Reynolds, P. Jadaun, J. T. Heron, C. L. Jermain, J. Gibbons, R. Collette, R. A. Buhrman, D. G. Schlom, and D. C. Ralph, Spin Hall torques generated by rare-earth thin films, Phys. Rev. B **95**, 064412 (2017).

[39] D. Lott Chen, A. Philippi-Kobs, M. Weigand, C. Luo, and F. Radu, Observation of compact ferrimagnetic skyrmions in $DyCo_3$ film, Nanoscale **12**, 18137 (2020).

[40] S. V. Stolyar, V. Y. Yakovchuk, I. G. Vazhenina, and R. S. Iskhakov, and J. Supercond, Study of surface anisotropy of

the interface of twolayer DyCo/FeNi films by the spinwave resonance method, Nov. Magn. **34**, 2969 (2021).

[41] W. Zhang, T. X. Huang, M. Hehn, G. Malinowski, M. Verges, J. Hohlfeld, Q. Remy, D. Lacour, X. R. Wang, G. P. Zhao, P. Vallobra, Y. Xu, S. Mangin, and W. S. Zhao, Optical creation of skyrmions by spin reorientation transition in ferrimagnetic CoHo alloys, ACS Appl. Mater. Interfaces **15**, 5608 (2023).

[42] N. Heiman and K. Lee, Magnetic properties of Ho-Co and Ho-Fe amorphous films, Phys. Rev. Lett. **33**, 778 (1974).

[43] K.-S. Lee, S.-W. Lee, B.-C. Min, and K.-J. Lee, Threshold current for switching of a perpendicular magnetic layer induced by spin Hall effect, Appl. Phys. Lett. **102**, 112410 (2013).

[44] T. Taniguchi, Theoretical condition for switching the magnetization in a perpendicularly magnetized ferromagnet via the spin Hall effect, Phys. Rev. B **100**, 174419 (2019).

[45] Y. Wang, P. Deorani, K. Banerjee, N. Koirala, M. Brahlek, S. Oh, and H. Yang, Topological surface states originated spin-orbit torques in Bi_2Se_3, Phys. Rev. Lett. **114**, 257202 (2015).

[46] A. K. Nayak, J. E. Fischer, Y. Sun, B. Yan, J. Karel, A. C. Komarek, C. Shekhar, N. Kumar, W. Schnelle, J. Kübler, and C. Felser, Large anomalous Hall effect driven by a nonvanishing Berry curvature in the noncolinear antiferromagnet Mn_3Ge, Sci. Adv. **2**, e1501870 (2016).

[47] F. Bonell, M. Goto, G. Sauthier, J. F. Sierra, A. I. Figueroa, M. V. Costache, S. Miwa, Y. Suzuki, and S. O. Valenzuela, Control of Spin−Orbit Torques by interface engineering in topological insulator heterostructures, Nano Lett. **20**, 5893 (2020).